

Transferability of vibrational normalizing-flow coordinates: A pathway towards intrinsic coordinates

Emil Vogt,^{1, a)} Álvaro Fernández Corral,^{1, 2} Yahya Saleh,^{1, 3} and Andrey Yachmenev^{1, 4, b)}

¹⁾ Center for Free-Electron Laser Science CFEL, Deutsches Elektronen-Synchrotron DESY, Notkestr. 85, 22607 Hamburg, Germany

²⁾ Department of Physics, Universität Hamburg, Luruper Chaussee 149, 22761 Hamburg, Germany

³⁾ Department of Mathematics, Universität Hamburg, Bundesstr. 55, 20146, Hamburg, Germany

⁴⁾ Center for Ultrafast Imaging, Universität Hamburg, Luruper Chaussee 149, 22761 Hamburg, Germany

(Dated: 2025-02-26)

Computing molecular vibrational energies and wavefunctions using variational approaches is a computationally demanding task, with the primary bottleneck being the diagonalization of the Hamiltonian matrix. The achievable accuracy depends on the dimensionality and complexity of the vibrational problem, the number and quality of the utilized basis functions and on the choice of vibrational coordinates. Composing basis sets with normalizing flows is a newly emerged idea to improve their expressivity and subsequently reduce the computational effort of variational methods. This approach generates coordinates tailored to a given vibrational problem for a selected truncated basis. We illustrate that the optimized coordinates results in more accurate predictions and faster convergence when transferred across different basis-set truncations, without the need for re-optimization. In addition, we show that the optimized coordinates are transferable across isotopologues and across molecules with similar structural motifs.

I. INTRODUCTION

Theoretical and computational studies of molecular vibrations are central to theoretical chemistry, molecular physics, and related scientific fields. Key areas of interest include the calculation and fitting of accurate potential energy surfaces (PESs)^{1–4}, the development of effective molecular Hamiltonians for efficient representations of molecular spectra^{5–7}, and the first-principles computation of accurate vibrational energies, wavefunctions, and spectra^{5, 7–9}. The latter can be accomplished with perturbation theory methods, variational theory approaches using finite-basis expansions, or pseudo-variational methods like discrete-variable representations. Central to all these methods is the construction of an appropriate vibrational Hamiltonian, which relies on carefully chosen coordinates and associated basis functions. The selection of coordinates plays an important role in defining the Hamiltonian operator, influencing the extent to which vibrational motions are coupled^{10, 11} and thus the overall computational efficiency. Determining an optimal coordinate system and compatible basis functions for describing molecular vibrations often requires substantial expertise and prior knowledge of the molecular vibrational behavior.

Rectilinear normal coordinates are effective for computing low-energy states in semi-rigid molecules, where the PES can be well-approximated by a low-order Taylor-series expansion around a single equilibrium geometry. However, these coordinates become inadequate in calculations of delocalized states, such as those encountered in floppy molecules^{12, 13}, or high-energy states in semi-rigid

molecules^{14, 15}, which sample larger and more complex regions of the phase space.

Curvilinear coordinates like Radau¹⁶, Jacobi^{17, 18}, valence¹⁹, ellipsoidal²⁰, hyperspherical²¹, and polyspherical^{22–24} types are often better suited for vibrational calculations in floppy molecules^{9, 25}. The optimal choice depends on the specific nuclear motions involved and requires an understanding of the morphology of the PES. Because vibrational motions vary widely across different molecular structures, no single coordinate system is universally optimal. The general approach for selecting effective coordinates is to capture the primary variations in the PES along individual dimensions, which helps to minimize coupling between different vibrational modes. Chemical intuition suggests that valence coordinates are most suitable for many molecules, as the localized electron density between adjacent atoms leads to significant changes in the PES with variations in bond lengths.

A promising strategy is to use general parametrized coordinates, with parameters optimized in variational calculations of vibrational energies. Optimized linear combinations of normal or valence coordinates have been explored in several studies^{20, 26–34}. While this approach has demonstrated a significant speed up in the basis-set convergence of energy calculations, it has not gained a widespread adoption. The primary reason is the insufficient speedup achieved in basis-set convergence through optimized linear coordinate mappings, which are overly restrictive, and the increased complexity introduced by the loss of symmetry inherent in such coordinate systems³⁵.

Once the vibrational coordinates have been selected, the next step is to choose an appropriate basis set, guided by the domain of each coordinate. For example, valence coordinates have domains of $[0, \infty)$ for bond lengths, $[0, \pi]$ for angles, and $[0, 2\pi]$ for dihedrals. A common approach is to use a direct-product basis of univariate orthogonal

^{a)}Email: emil.vogt@cfel.de

^{b)}Email: andrey.yachmenev@cfel.de;

URL: <https://www.controlled-molecule-imaging.org>

polynomial-based functions (or their linear combinations), primarily due to their close relation with Gaussian quadratures^{13,36}. This approach simplifies the evaluation of integrals necessary for the calculation of the Hamiltonian matrix elements and facilitates transformations between the finite-basis representations and their corresponding discrete-variable representations. The specific univariate functions are chosen based on the coordinate domain, the shape of the PES along the coordinate, and the degree of vibrational coupling in the Hamiltonian.

In electronic structure problems, neural networks have been successfully used to represent eigenfunctions for the ground and few lowest excited states^{37,38}. However, while these methods have demonstrated notable accuracy for ground states, their accuracy and efficiency in excited-state calculations remains considerably lower. The performance also diminishes as the number of target excited states increases. This limitation reduces the current utility of neural-network representations of wavefunctions for vibrational problems, as these often require the computation of hundreds or even thousands of highly accurate excited states.

We recently introduced a new approach for nonlinear parametrization of vibrational coordinates based on normalizing flows^{39,40}, implemented through an invertible residual neural network⁴¹. In this method, the neural network parameters are optimized using the variational principle to minimize the approximate energies. Unlike traditional approaches - where basis functions are selected only after the coordinates are defined - the normalizing-flows approach optimizes the coordinates to maximize the performance of a chosen truncated basis set, tailoring it to the specific application.

In this work, we show that the specificity of normalizing-flows vibrational coordinates does not constrain their broader applicability. Specifically, we demonstrate the transferability of normalizing-flow coordinates, originally optimized for a molecule with a small number of basis functions, to other calculations without re-optimization or with only minor adjustments. This includes their application across different basis set truncations, isotopologues, and to molecules with similar structural motifs (X_2Y , demonstrated here for $H_2S \rightarrow H_2O$). For all three categories, normalizing-flow coordinates demonstrate superior performance as compared with conventional curvilinear valence-bond coordinates.

The significance of these findings is twofold. First, the normalizing-flows approach facilitates the transfer of knowledge about optimal coordinates to related systems, thereby improving computational efficiency by providing a suitable initial guess for subsequent optimizations. Second, the generality of these results across different molecules can potentially advance our understanding of intrinsic coordinates, i. e., coordinates that most naturally capture the motion of vibrations, in diverse systems. We discuss why normalizing-flow coordinates are particularly effective and provide illustrative examples to aid the interpretation of results obtained with this new category

of vibrational coordinates. We focus primarily on hydrogen sulfide H_2S and its deuterated isotopologues, and refer the reader to Saleh *et al.*³⁹ for initial applications of normalizing-flow coordinates for H_2CO and HCN/CNH . Normalizing-flow coordinates have also been used in conjunction with Monte-Carlo integration to approach larger molecular systems, such as CH_3CN and C_2H_4O ⁴², and to investigate anharmonic effects in lithium solids at finite temperatures⁴³.

II. THEORY

In variational basis representations, the vibrational Schrödinger equation,

$$\hat{H}\Psi_n = (\hat{T} + \hat{V})\Psi_n = E_n\Psi_n, \quad (1)$$

where Ψ_n and E_n are the n -th eigenfunction and eigenvalue, respectively, is projected onto a finite set of orthonormal basis functions. The vibrational eigenfunctions, Ψ_n ($n = 0 \dots N - 1$), are approximated as linear combinations of M basis functions $\{\phi\}_{m=0}^{M-1}$, with $M \geq N$, as

$$\Psi_n(\mathbf{r}) \approx \tilde{\Psi}_n(\mathbf{r}) = \sum_{m < M} c_{nm}\phi_m(\mathbf{r}), \quad (2)$$

where \mathbf{r} denotes the vibrational coordinates.

By introducing this linear expansion into the weak formulation of the Schrödinger equation, one obtains a matrix eigenvalue problem

$$\mathbf{H}\mathbf{C} = \mathbf{E}\mathbf{C}, \quad (3)$$

where $\mathbf{H} = \{\langle\phi_m|\hat{H}|\phi'_m\rangle\}_{m,m'=0}^{M-1}$ is the Hamiltonian matrix, $\mathbf{C} = \{c_{mn}\}_{m=0, n=0}^{M-1, N-1}$ are the linear expansion coefficients, and $\mathbf{E} = \{E_n\}_{n=0}^{N-1}$ are the approximated vibrational energies. The accuracy of calculated energies can be systematically improved by increasing the number of basis functions M , ensuring variational convergence to the true energies as lower bound. In practice, quadratures or truncated Taylor-series expansions are often employed to evaluate the integrals required to construct the Hamiltonian matrix elements, which introduce additional errors to the truncated basis representation and may even result in a violation of the variational principle.

An alternative approach to systematically improve calculated energies is to enhance the approximation power of the chosen basis functions. To achieve this, we start with a truncated set of orthonormal basis functions $\{\phi_m(\mathbf{q})\}_{m=0}^{M-1}$ defined on a coordinate set \mathbf{q} . The coordinate set \mathbf{q} is related to an initial set of vibrational coordinates \mathbf{r} through a parametrized invertible mapping f_θ , such that $\mathbf{q} = f_\theta(\mathbf{r})$. Because the mapping is invertible, the reverse relation also holds, $\mathbf{r} = f_\theta^{-1}(\mathbf{q})$. The augmented basis functions are then defined as

$$\gamma_m(\mathbf{q}; \theta) = \phi_m(\mathbf{q})\sqrt{D}, \quad (4)$$

where $D = |1/\det(\nabla_{\mathbf{q}}f_{\theta}^{-1}(\mathbf{q}))|$ is the absolute value of the inverse of the determinant of the Jacobian. The inclusion of the factor \sqrt{D} ensures that the augmented basis functions remain orthonormal, regardless of the values of parameters θ . These basis functions can also be evaluated in the vibrational coordinates \mathbf{r} as $\gamma_m(f_{\theta}(\mathbf{r});\theta)$.

In principle, the mapping f_{θ} can be any differentiable invertible function. However, for the augmented basis set to remain complete, the normalizing flow must satisfy the bi-Lipschitz condition⁴⁴. This means that there exist constants $k, K > 0$ such that $k \leq 1/|\det(\nabla_{\mathbf{q}}f_{\theta}^{-1}(\mathbf{q}))| \leq K$ for all \mathbf{q} within the domain. We implement f_{θ} as an invertible residual neural network (iResNet)⁴¹, which is bi-Lipschitz by construction.

By applying the coordinate transformation $\mathbf{q} = f_{\theta}(\mathbf{r})$ in integrals, we can express the matrix elements of the vibrational kinetic and potential energy operators within the augmented basis (4). For the potential energy, this leads to the expression:

$$\begin{aligned} \mathbf{V}_{mm'} &= \int \phi_m^*(f_{\theta}(\mathbf{r}))\sqrt{D} V(\mathbf{r})\phi_{m'}(f_{\theta}(\mathbf{r}))\sqrt{D} d\mathbf{r} \quad (5) \\ &= \int \phi_m^*(\mathbf{q})V(f_{\theta}^{-1}(\mathbf{q}))\phi_{m'}(\mathbf{q}) d\mathbf{q}, \end{aligned}$$

where the volume elements of integrations are related by $d\mathbf{q} = D d\mathbf{r}$. This formulation shows how the change of coordinates effectively modifies the operators within matrix elements in the original basis set $\{\phi_m\}_{m=0}^{M-1}$. Consequently, optimizing f_{θ} for enhancing the expressivity of basis functions in (4) is equivalent to optimizing the coordinates, in which the Hamiltonian operator within the chosen fixed basis set is expressed.

The corresponding expression for the kinetic energy matrix elements after the coordinate transformation is

$$\begin{aligned} T_{mm'} &= \int \phi_m^*(f_{\theta}(\mathbf{r}))\sqrt{D} \hat{T}(r) \phi_{m'}(f_{\theta}(\mathbf{r}))\sqrt{D} d\mathbf{r} \quad (6) \\ &= \frac{\hbar^2}{2} \sum_{kl} \int \left[\left(\frac{1}{2\sqrt{D}} \frac{\partial D}{\partial q_k} + \sqrt{D} \frac{\partial}{\partial q_k} \right) \phi_m^*(\mathbf{q}) \right] \\ &\quad \sum_{\lambda\mu} \frac{\partial q_k}{\partial r_{\lambda}} G_{\lambda\mu}(f_{\theta}^{-1}(\mathbf{q})) \frac{\partial q_l}{\partial r_{\mu}} \\ &\quad \left[\left(\frac{1}{2\sqrt{D}} \frac{\partial D}{\partial q_l} + \sqrt{D} \frac{\partial}{\partial q_l} \right) \phi_{m'}(\mathbf{q}) \right] d\mathbf{q}, \end{aligned}$$

where $G_{\lambda\mu}$ are the elements of the mass-weighted metric tensor (Wilson G -matrix). In addition, the pseudo-potential term,

$$V' = \frac{\hbar^2}{32} \sum_{\lambda} \sum_{\mu} \frac{G_{\lambda\mu}}{\tilde{g}^2} \frac{\partial \tilde{g}}{\partial r_{\lambda}} \frac{\partial \tilde{g}}{\partial r_{\mu}} + 4 \frac{\partial}{\partial r_{\lambda}} \left(\frac{G_{\lambda\mu}}{\tilde{g}} \frac{\partial \tilde{g}}{\partial r_{\mu}} \right), \quad (7)$$

where $\tilde{g} = \det(\mathbf{G}^{-1})$, also contributes to the exact kinetic energy operator. The pseudo-potential arises from the original coordinate transformation from Cartesian to the

initial internal coordinates \mathbf{r} . As a scalar function of the vibrational coordinates, matrix elements involving the pseudo-potential can be evaluated analogously to the potential energy operator in (5).

A. Invertible Neural Networks

To model the normalizing flow f_{θ} , we used an iResNet consisting of 10 blocks (five blocks for the one-dimensional example, *vide infra*). An iResNet is given by concatenating blocks of the form

$$\mathbf{x}_{k+1} = \mathbf{x}_k + \mathbf{h}_k(\mathbf{x}_k; \theta), \quad (8)$$

where \mathbf{x}_k is the input to the block and $\mathbf{h}_k(\mathbf{x}; \theta)$ is a feed-forward neural network composed of weights, biases and nonlinear activation functions. In this work, each block was constructed as a dense neural network with two hidden layers with unit sizes [8, 8], and an output layer with the number of units equal to the number of coordinates. A block is guaranteed to be invertible if it has a Lipschitz constant of < 1 . The inverse of each block was obtained by a fixed-point iteration algorithm.

To guarantee that the feed-forward networks \mathbf{h}_k for $k = 0, \dots, K-1$ satisfy the aforementioned Lipschitz condition, we used the LipSwish activation function

$$\sigma(x) := \frac{x}{1.1} \frac{1}{1 + \exp(-x)}, \quad (9)$$

which has a Lipschitz constant of ~ 1 . With this activation function, the block \mathbf{h}_k is guaranteed to be Lipschitz if each of its weight matrices, \mathbf{W} , has a spectral norm of < 1 . This is achieved by setting

$$\mathbf{W} = \begin{cases} \mathbf{W} & \text{if } \|\mathbf{W}\|_2 < c \\ \mathbf{U}\tilde{\Sigma}\mathbf{V}^T & \text{if } \|\mathbf{W}\|_2 \geq c, \end{cases}$$

where $0 < c < 1$ is a hyperparameter, $\|\mathbf{W}\|_2$ is the spectral norm of the weight matrix \mathbf{W} , \mathbf{U} and \mathbf{V} are the left and right singular vectors of \mathbf{W} , respectively, and $\tilde{\Sigma}$ is a matrix containing the corresponding modified singular values,

$$\tilde{\Sigma}_{ii} = \begin{cases} \Sigma_{ii} & \text{if } \Sigma_{ii} < c \\ c & \text{if } \Sigma_{ii} \geq c. \end{cases}$$

A hyperbolic tangent wrapper was applied to the output of the inverse pass of the iResNet (input of the forward pass), $\mathbf{x}_K \rightarrow \tanh(\mathbf{x}_K)$, which maps all dimensions to a domain of $[-1, 1]$. The final output of the inverse pass was linearly scaled from the range $[-1, 1]$ to match the domain of the original vibrational coordinates:

$$f_{\theta}^{-1}(\mathbf{x}) = \mathbf{a} \cdot \tilde{f}^{-1}(\mathbf{x}) + \mathbf{b}. \quad (10)$$

This ensures that $f_{\theta}^{-1}(\mathbf{x})$ is contained within the original coordinate domain for all possible θ .

B. Loss Function

To optimize the parameters θ of f_θ , we take advantage of the variational principle to define the loss function as

$$\mathcal{L}_\theta^M = \sum_{n < M} E_n \rightarrow \min_\theta. \quad (11)$$

If the number of target states is equal to the number of basis functions, $M = N$, this loss function can be efficiently computed as $\mathcal{L}_\theta^N = \text{Tr}(\mathbf{H})$, eliminating the need to calculate off-diagonal matrix elements of the Hamiltonian matrix. Despite the added complexity, the computational cost of calculating off-diagonal matrix elements and repeated Hamiltonian matrix diagonalization can be justified when the optimization focuses on a specific subset of states of interest. In such cases, focusing on a smaller set of eigenvalues and selectively improving their accuracy can lead to a more efficient and targeted optimization process.

The loss function was optimized using the `Optax`⁴⁵ Adam optimizer with a learning rate of 0.001, $\beta_1 = 0.9$, $\beta_2 = 0.999$, $\epsilon = 10^{-8}$, and $\bar{\epsilon} = 0.0$.

C. A One-dimensional Motivating Example

To better understand the morphology and effectiveness of the normalizing-flows coordinate optimization, we examine its application to a typical one-dimensional example of molecular vibrations: the Morse oscillator⁴⁶. The Hamiltonian for the Morse oscillator is

$$H_M(x) = \frac{-\hbar^2}{2\mu} \frac{\partial^2}{\partial x^2} + D_e [1 - \exp(-a_M x)]^2, \quad (12)$$

where μ is the reduced mass of the oscillator, D_e is the dissociation energy, a_M is a second Morse parameter, and $x = r - r_e$ is the displacement coordinate relative to the equilibrium bond distance, r_e . The nonlinear coordinate transformation $z = 1 - \exp(-a_M x)$ maps the Morse potential into a harmonic potential,

$$V_M(x) = D_e [1 - \exp(-a_M x)]^2 \rightarrow \tilde{V}(z) = D_e z^2. \quad (13)$$

It may seem that the Hermite functions - eigenfunctions of the harmonic oscillator - could be used to exactly solve the problem. However, this coordinate transformation also modifies the kinetic energy operator. Specifically, the change in the volume element $dx \rightarrow dz$ results in the following kinetic energy operator expressed in the z coordinate

$$\tilde{T}(z) = \frac{-\hbar^2}{2\mu} \left(\alpha \frac{\partial^2}{\partial z^2} + \beta \frac{\partial}{\partial z} + \gamma \right), \quad (14)$$

with $\alpha = a_M^2(1-z)^2$, $\beta = -2a_M(1-z)$, and $\gamma = \frac{a_M^2}{4}$. This expression differs from the standard kinetic energy operator for both the Morse and harmonic oscillators.

It is therefore not possible to map the Morse-oscillator Hamiltonian into the harmonic-oscillator Hamiltonian by a change of coordinates. This limitation can also be realized from the fact that a coordinate transformation does not change relative positions of nodes between different basis functions. For example, the odd harmonic-oscillator eigenfunctions share a node at $x = 0$, the eigenfunctions of the Morse oscillator do not. In addition, the transformed coordinate z is defined in the domain $(-\infty, 1)$, which is incompatible with the domain $(-\infty, \infty)$ required for harmonic-oscillator eigenfunctions.

The optimal coordinate transformation can be determined by minimizing the loss function in (11). As demonstrated, this transformation does not establish a one-to-one correspondence between the Hermite basis functions and the Morse-oscillator eigenfunctions. Instead, the optimal transformation ensures that the span of the N Morse-oscillator eigenfunctions of interest, $\{\Psi(\mathbf{r})\}_{n=0}^{N-1}$, is optimally captured within the span of the M augmented harmonic-oscillator basis functions, $\{\gamma(f_\theta(\mathbf{r}); \theta)\}_{m=0}^{M-1}$.

We optimized linear and nonlinear coordinate transformations in the variational solution of the Morse-oscillator problem. The potential parameters used were $a_M = 2.1440 \text{ \AA}^{-1}$, $D_e = 42301 \text{ cm}^{-1}$, representative of a typical OH-stretching mode in molecules⁴⁷. Both coordinate transformations were optimized to approximate all 23 bound states using a basis of 23 Hermite functions. The normalizing-flows transformation was modelled by the iResNet with five residual blocks (see Section II A), which proved sufficient to achieve convergence of the coordinates. The Morse potential expressed in fixed (*vide infra*) and optimized linear and normalizing-flow coordinates are shown in FIG. 1. In both of the optimized coordinates, the Morse potential is shifted relative to the Hermite basis reference at $x = 0$, positioning the basis center closer to the average density center of the eigenstates, $r_0 = \frac{1}{N} \sum_n \langle \Psi_n | r | \Psi_n \rangle$. This shift indicates that the optimal mapping is not a direct one-to-one correspondence between the Hermite basis functions and the Morse-oscillator eigenfunctions, $\gamma_n \rightarrow \Psi_n$. As a result, the largest contribution to the n -th eigenstate does not necessarily come from the n -th basis function.

The computed energy values for the Morse-oscillator problem expressed in fixed linear, optimized linear, and normalizing-flow coordinates are presented in Table I. The parameters a and b for the fixed linear coordinates are derived from a quadratic expansion of the potential in x , followed by mapping of the resulting Hamiltonian onto the harmonic oscillator Hamiltonian. This yields,

$$a = \left(\frac{F}{\mu \hbar^2} \right)^{1/4}, \quad b = 0, \quad (15)$$

where $F = \frac{d^2 V(x)}{dx^2}|_{x=0}$ is the force constant. The fixed linear transformation is most effective for the lowest energy states, where wavefunctions remain largely confined within the region where the quadratic expansion of the potential holds. However, its accuracy declines rapidly with

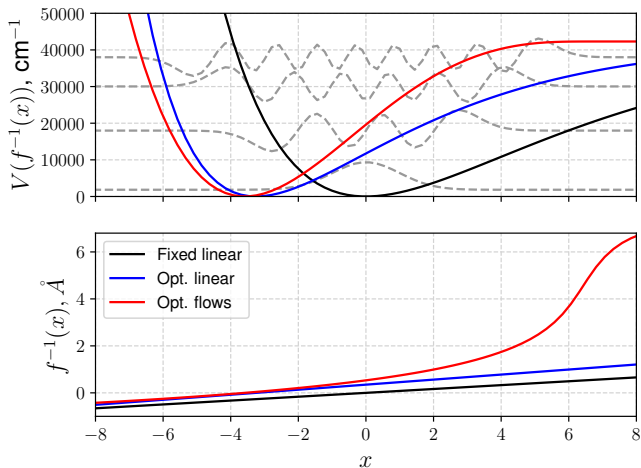


FIG. 1. (Top panel) Morse potential expressed in fixed linear coordinates (black), optimized linear coordinates (blue) and normalizing-flow coordinates (red). The Hermite functions, $\mathcal{H}_n(x)$, with $n = 0, 5, 10, 15$ are depicted as grey dashed lines. (Bottom panel) The corresponding coordinate transformations.

increasing level of excitation. In contrast, optimized linear coordinates perform worse for the lowest energy states but degrade more gradually with increasing level of excitation. Normalizing-flow coordinates offer significantly improved accuracy across all energy levels, demonstrating the advantages of nonlinear coordinate transformations.

The linear parameters in (15) provide a well-established approach for modifying the coordinate mapping in response to changes in physical parameters of the system (e. g., μ or F). However, the corresponding mapping strategy for the normalizing-flow coordinates is not entirely clear. To address this, in Section III B we investigate the transferability of the optimized normalizing-flow coordinates in isotopologues, i. e., molecules that share the same structure but differ in nuclear masses.

D. Details of Multidimensional Calculations

For the multidimensional calculations on H_2S and H_2O , the reference vibrational coordinates were chosen as conventional displacement-based valence coordinates, i. e., bond lengths and angles. Multidimensional basis functions were expressed as direct products of Hermite basis functions in all examples. The normalizing-flows architecture enables mapping of any input coordinate range, defined by the domain of \mathbf{q} (optimized coordinates), to any output coordinate range, defined by the domain of \mathbf{r} (initial valence coordinates). Therefore, Hermite basis functions are suitable for both the bond stretching coordinates, $(-\infty, \infty) \rightarrow [0, \infty)$, and the angular coordinates, $(-\infty, \infty) \rightarrow [0, \pi]$, provided that the boundary conditions $\Psi_m \rightarrow 0$ and $\frac{\partial \Psi_m}{\partial q} \rightarrow 0$ are satisfied for all m of interest.

The direct-product basis was truncated by including

State	Fixed linear	Opt. linear	Opt. flows	Reference
0	1838.973	1839.060	1838.973	1838.973
1	5394.319	5395.019	5394.319	5394.319
2	8786.199	8792.357	8786.199	8786.199
3	12014.61	12049.57	12014.61	12014.61
4	15079.57	15179.36	15079.56	15079.56
5	17981.52	18155.42	17981.04	17981.04
6	20728.82	20982.55	20719.06	20719.06
7	23388.67	23732.85	23293.61	23293.61
8	26163.27	26416.76	25704.69	25704.69
9	29264.49	28966.13	27952.31	27952.31
10	32765.44	31315.58	30036.47	30036.46
11	36686.37	33429.37	31957.18	31957.14
12	40993.55	35297.63	33714.47	33714.36
13	45781.41	36900.91	35308.38	35308.11
14	51111.91	38389.79	36738.93	36738.40
15	56489.49	39614.34	38006.14	38005.22
16	63550.75	41484.32	39110.04	39108.57
17	76662.53	43077.35	40050.60	40048.46
18	99098.51	45237.53	40827.66	40824.88
19	134083.8	47989.70	41440.98	41437.83
20	187873.2	49875.60	41890.97	41887.32
21	273469.8	55280.78	42178.18	42173.35
22	425156.5	57058.45	42307.43	42295.90
Sum	1684363.7	716460.43	652331.80	652300.37

TABLE I. Calculated bound state energy levels (in cm^{-1}) for the Morse potential using a basis of 23 Hermite functions. Results are provided for fixed linear, optimized linear, and normalizing-flows coordinate transformations. The reference energy levels were calculated analytically.

only basis-product configurations (n_1, n_2, n_3) that satisfy the polyad condition $2n_1 + 2n_2 + n_3 \leq P_{\text{max}}$, where n_1 , n_2 , and n_3 represent the Hermite basis function indices corresponding to the two stretching and one bending valence coordinate, respectively.

The PES used for H_2S and its isotopologues was obtained from Azzam *et al.*⁴⁸, while the PES for H_2O was taken from Conway *et al.*⁴⁹.

III. RESULTS & DISCUSSION

A. Transferability Across Basis-Set Truncations

During the training of normalizing-flow mapping, the neural network leverages all available information from the truncated basis set to enhance its performance. As a consequence, the training process disregards the functions in the basis set that are not used in the approximation. This might suggest that the results of the optimal coordinate mapping depend strongly on the number of employed basis functions during training. However, due to the inherent property of normalizing flows preserving the completeness and orthogonality of the basis set (in our case - Hermite functions), the optimal coordinate mapping appears to be largely independent of the number of basis functions

N , provided a reasonable basis set is used for training.

The computational cost of the training process scales with the number of basis functions, N , as N^3 , if the loss function involves solving an eigenvalue problem, in addition to scaling with the complexity of the neural network. The approximate independence of normalizing flows from the number of basis functions enables an efficient training protocol. In this approach, the normalizing-flow coordinates are first optimized using a small or intermediate number of basis functions and can then be transferred to sets employing more basis functions for higher accuracy in energy calculations.

In FIG. 2, we show the convergence for the 100 first energy levels of H_2S with respect to the basis-set truncation parameter, defined by the maximal polyad number P_{\max} . The results are obtained using fixed linear, optimized linear, and optimized normalizing-flow coordinate mappings. The fixed linear mapping was computed for each coordinate using the expression (15). Two types of normalizing-flows mappings are compared: those optimized for each specific P_{\max} and those optimized for selected values of P_{\max} (12, 16, 20) and subsequently transferred to calculations with larger P_{\max} . The metric for the convergence is the error of the individual energy levels ($E_i - E_i^{(\text{Ref})}$), where the reference energy levels were computed using a basis set truncated at $P_{\max} = 60$ with normalizing flows optimized for $P_{\max} = 28$. To minimize quadrature errors in the computed reference energy levels, a direct-product quadrature scheme was employed, using 121-point Gauss-Hermite quadrature in each dimension.

As illustrated in FIG. 2, coordinate optimization significantly improves the accuracy of computed energy levels. Using normalizing-flow coordinates, this improvement reaches up to approximately eight orders of magnitude compared to the fixed linear scaling of standard valence coordinates. When the linear scaling parameters are optimized, the improvement is still significant, at about five orders of magnitude. To achieve the convergence of the same significant numbers obtained with 140 and 1240 basis functions using normalizing-flow coordinates, approximately 2500 and 67000 basis functions would be required with valence coordinates, respectively. When the linear scaling parameters are optimized, these numbers reduce to 450 and 6200. FIG. 2 also clearly demonstrates the increased convergence rate of calculations as a function of the number of basis functions.

In addition, FIG. 2 illustrates that the energies calculated using transferred normalizing-flow coordinates remain significantly more accurate than those obtained with linearly scaled valence coordinates, even when the linear scaling parameters are optimized for the calculation at hand. For calculations using basis sets $P_{\max} = 24$ and 28, flow coordinates, optimized at $P_{\max} = 12, 16$, and 20, yield comparable results, with slight improvements as P_{\max} increases, as expected. This demonstrates the efficiency of transferring flow coordinates from smaller to calculations employing more basis functions without additional optimization.

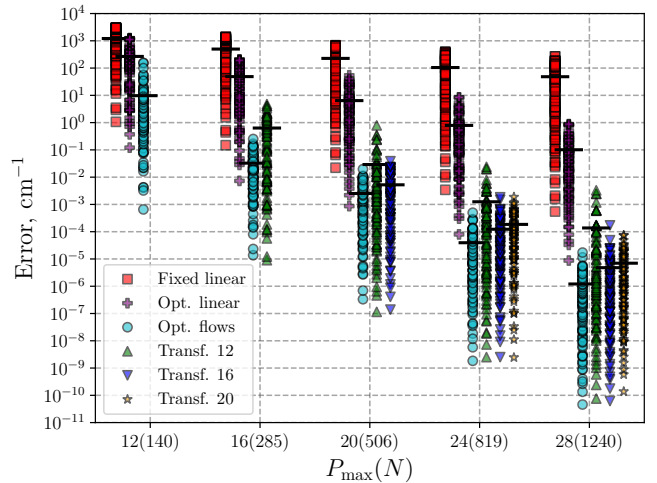


FIG. 2. Convergence of the first 100 energy levels of H_2S using fixed linear (red squares), optimized linear (purple plus signs), and optimized normalizing-flows (cyan circles) coordinate mappings. Results are plotted for different numbers of basis functions, defined by the maximal polyad number P_{\max} , with the corresponding number of basis functions, N , indicated in parentheses. Additionally, results obtained with normalizing-flows mappings optimized for $P_{\max} = 12$ (green up-triangles), $P_{\max} = 16$ (blue down-triangles), and $P_{\max} = 20$ (orange stars) and applied to calculations with larger P_{\max} are included. Thick horizontal lines indicate the average energy-level error for each P_{\max} , whose minimization is the objective of the training process. Data points are slightly offset along the P_{\max} axis for improved visual clarity.

The convergence of the approximation using the Hermite basis with respect to the number of functions, N , is exponential⁵⁰, $\|\Psi_n - \hat{\Psi}_n\| < A N^{-k}$, where $\|\cdot\|$ refers to the L^2 norm, A is a constant that depends on the relation of the target function to the operators associated to the basis, and k is the convergence rate. The convergence for the Hermite basis defined in normalizing-flow coordinates is also exponential⁵¹, with different constants A and k for each map. Therefore, it is reasonable to assume that the loss function defined in (11) converges exponentially fast, i. e.,

$$\mathcal{L}(N) = \frac{\mathcal{L}_\theta^{100}(N) - \mathcal{L}_{\text{Ref}}^{100}}{100} \sim A N^{-k}, \quad (16)$$

where θ are the optimized parameters for the chosen N . To quantify the improved convergence rate observed for the normalizing-flow coordinates (see FIG. 2), we fitted $\log(\mathcal{L})$ with a linear expression in N , i. e., $\log(\mathcal{L}) = -k \log(N) + \log(A)$. The regression parameters derived from this fit are shown in Table II. The convergence rate of both of flows-related coordinates is significantly better than any linear method. Remarkably, the convergence rate of transferred normalizing-flow coordinates is better than that of optimized linear parameters at each truncation, without the need for any reoptimization. This supports the use of transferred coordinates

for accurate calculations with a large number of basis functions. The constant A is also decreased by the use of nonlinear coordinates, which means that the accuracy is improved for any fixed truncation.

Coordinate	$k \times 10^3$	$\log(A)$
Fixed linear	0.61 ± 0.08	11.7 ± 0.3
Opt. linear	1.53 ± 0.15	10.6 ± 0.5
Opt. flows	2.90 ± 0.47	6.43 ± 2
Transf. flows	2.17 ± 0.30	7.11 ± 1

TABLE II. Fitted convergence parameters for different coordinate mappings. The transferred flows coordinate was optimized for $P_{\max} = 12$.

The substantial improvement in basis set convergence achieved with normalizing-flow coordinates compared to valence coordinates significantly reduces computational effort. For example, converging first 100 energies of H_2S to errors below 10^{-5} cm^{-1} on average requires approximately $(67000/1240)^3 \approx 50^3 = 125\,000$ times less computational effort. Thus, the transferability of flow coordinates across basis-set truncations also highlights their practical utility for higher-dimensional systems, offering a promising potential for future applications.

For a direct-product basis of univariate basis functions, we attribute the improved accuracy of energy predictions achieved with normalizing flows to two primary factors. First, the increased mode-separability of the Hamiltonian³⁹ accelerates convergence, as the eigenfunctions of a perfectly separable Hamiltonian can be expressed as direct products of eigenfunctions corresponding to each vibrational degree of freedom. Second, optimal coordinates modify the Hamiltonian along each individual dimension such that the one-dimensional eigenfunctions can be best expressed by their respective univariate basis functions, which is illustrated by the improved localization of density in Section II C. According to this interpretation, intrinsic vibrational coordinates cannot be defined independently of the reference basis underlying the expansion of the vibrational wavefunctions in the solution of the Schrödinger equation. With respect to the chosen basis, the normalizing-flow coordinates act as intrinsic vibrational coordinates.

B. Transferability Across Isotopologues

In the previous section, we demonstrated the transferability of optimized normalizing-flow coordinates across different basis-set truncations, a property that has also been tested for other molecules, such as H_2CO and HCN/CNH ³⁹. Additionally, we showed that normalizing flows produce interpretable and physically meaningful coordinate mappings³⁹. This naturally suggests that normalizing flows optimized for solution of the nuclear Schrödinger equation may inherently learn coordinates in-

trinsic to the vibrations of molecules with similar chemical structures.

In this section, we explore this hypothesis by investigating the effectiveness of transferring flow coordinates between isotopologues of H_2S . Specifically, we first optimized the coordinates in variational calculations for the lowest 100 vibrational energy levels of H_2S using a basis set truncated at $P_{\max} = 12$. The optimized coordinates were subsequently applied to calculations of the vibrational energy levels of D_2S and HDS .

A direct comparison of the energies obtained with the transferred flow coordinates and those calculated with fixed linear transformation of valence coordinates is shown in FIG. 3. In contrast to the transferred flow coordinates, the fixed linear transformation inherently accounts for mass changes when applied to different isotopologues. Overall, the transferred flow coordinates yield more accurate energy levels compared to the valence coordinates, with the largest error reduction being about three orders of magnitude. The transferred flow coordinates also show faster convergence with respect to the basis-set truncation P_{\max} . This improvement in accuracy is more pronounced for HDS compared to D_2S , particularly for lower vibrational levels, which are generally better converged with fixed linear valence bond coordinates. We attribute this improved performance to the enhanced separability of the Hamiltonian when expressed in flow coordinates³⁹.

Enhanced separability implies that the energy levels can be more accurately approximated as a sum of contributions from individual vibrational modes. However, when isotopic substitutions are made, such as transitioning from H_2S to HDS , the Hamiltonian separability decreases slightly. In such cases, the transferred flow coordinates can still provide reasonably accurate energy predictions for low-energy states, although their accuracy diminishes for higher-energy states. When two isotopic substitutions are made, as in the transition from H_2S to D_2S , the Hamiltonian becomes even less separable. As a result, the transferred coordinates are less effective, leading to reduced accuracy in predicting energy levels, even for the low-energy states.

To further improve the performance of the transferred flow coordinates, we fine-tuned the linear model parameters \mathbf{a} and \mathbf{b} in (10). For D_2S and HDS , this refinement involved solving the Schrödinger equation for 100 vibrational states, using only 40 iterations with the Adam optimizer. The results for the fine-tuned coordinates in FIG. 3 show a significant improvement of computed energy levels by up to more than three orders of magnitude compared to the fixed linear transformation of valence coordinates.

The fine-tuning process for transferred coordinates across isotopologues is well-founded, as the fixed linear mapping of valence coordinates already includes mass-dependent parameters (see (15)). Based on this fixed linear mapping, the variation in the linear parameters of the normalizing-flow model is expected to scale proportionally to the diagonal elements of the mass-weighted

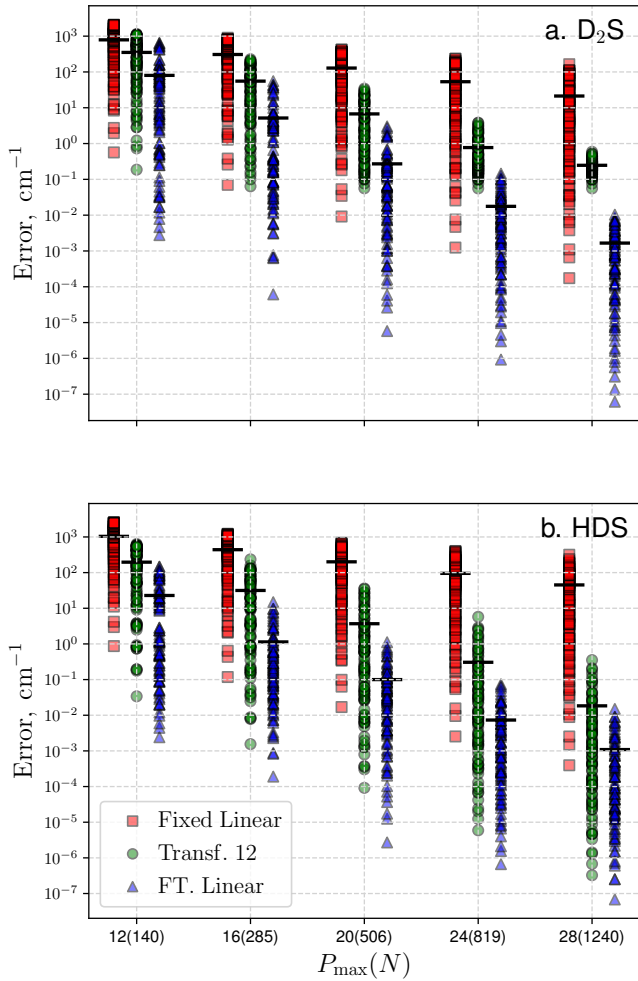


FIG. 3. Convergence of the first 100 vibrational energy levels of (a) D_2S and (b) HDS using fixed linear transformation of valence coordinates (red squares), transferred normalizing-flow coordinates (green circles), and fine-tuned transferred normalizing-flow coordinates (blue triangles). The vertical axis represents the calculated energy error, $E_i - E_i^{(\text{Ref})}$, while the horizontal axis shows the basis-set truncations, P_{max} . The transferred coordinates were originally optimized for H_2S with $P_{\text{max}} = 12$, and the fine-tuned parameters were obtained through re-optimization of the linear parameters in the normalizing-flows model. The black horizontal lines show the average error per energy level. The data points are slightly offset along the P_{max} axis for visual clarity.

metric tensor, i.e., $a_i \propto G_{ii}^{-1/4}$. Likewise, $b_i \rightarrow 0$ as $G_{ii} \rightarrow 0$ is expected based on the eigenstate average density center argument presented in Section II C. Non-Born-Oppenheimer effects are not considered, and the PES is therefore approximated to be invariant across isotopologues.

C. Transferability Across Molecules

Conventional geometrically defined curvilinear coordinates are broadly applicable across various molecules. For example, valence coordinates are particularly well suited for semi-rigid molecules like H_2S , H_2O and H_2CO , and can be conveniently expressed using a Z-matrix representation. In the previous section, we demonstrated the universality of optimized normalizing-flow coordinates across isotopologues. Here, we extend this analysis to evaluate the performance of flows coordinates when transferred between different molecules with similar chemical structures.

In FIG. 4, we compare the convergence of the first 100 vibrational energy levels of H_2O for $P_{\text{max}} = 12$, computed using fixed linear combinations of valence coordinates and flow coordinates optimized for H_2S with $P_{\text{max}} = 12$. The results show that the normalizing-flow coordinate transferred from H_2S to H_2O yield better predictions for all 100 energy levels compared to the valence coordinates. This demonstrates the utility of knowledge transfer between the Hamiltonians of H_2S and H_2O . The observed improvement is perhaps not surprising, given the morphological similarity of their PESs, as reflected by the shared applicability of valence coordinates to both systems. Consequently, the flow coordinates optimized for H_2S appear to serve as more intrinsic coordinates for H_2O , within the chosen direct-product basis of Hermite functions.

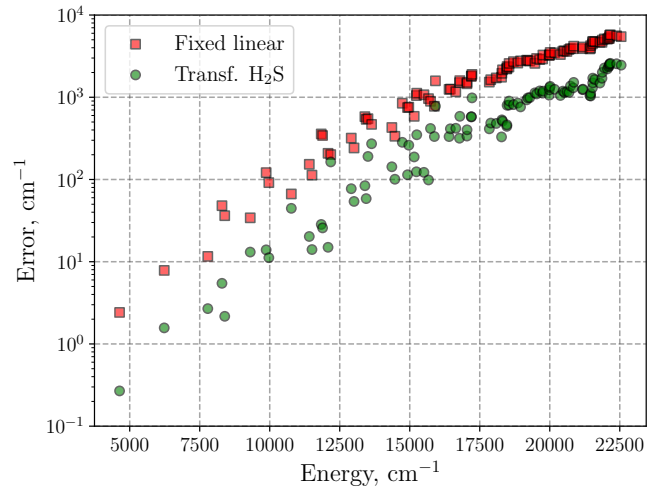


FIG. 4. Convergence of the first 100 energy levels of H_2O for $P_{\text{max}} = 12$ using fixed linear transformed valence coordinates (red squares) compared to normalizing-flow coordinates transferred from H_2S calculations with $P_{\text{max}} = 12$ (green circles). The vertical axis represents the calculated energy error, $E_i - E_i^{(\text{Ref})}$, while the horizontal axis shows the reference energy, $E_i^{(\text{Ref})}$. The converged energy values for H_2O were computed using optimized flow coordinates with $P_{\text{max}} = 24$.

IV. CONCLUSION

The normalizing flow approach provides a versatile framework for optimizing vibrational coordinates in variational calculations of molecular vibrational energies. In previous work, we showed that optimized flow coordinates produce physically meaningful transformations, enhancing the separability of the Hamiltonian when expressed in a direct-product basis³⁹.

A key question is whether the normalizing-flows method can learn intrinsic coordinates that not only improve computational performance for individual molecules, but also generalize effectively to other molecules and broader applications in computational chemistry. We took an initial step toward addressing this challenge. We demonstrated that optimizing vibrational coordinates using normalizing flows can dramatically improve the accuracy of variationally computed vibrational energies by several orders of magnitude. Furthermore, these coordinates significantly enhance basis-set convergence rates compared to both fixed linear and optimized linear transformations of valence coordinates.

While the normalizing-flow coordinates are optimized for a specific molecule, truncated basis set, and target set of states, our findings demonstrate that this specificity does not constrain their broader applicability. Optimized flow coordinates can be transferred effectively across basis-set truncations, isotopologues, and even to different molecules as demonstrated for $\text{H}_2\text{S} \rightarrow \text{H}_2\text{O}$. The transferability across basis truncations makes the method particularly cost-effective, enabling efficient scaling of computations to discretizations employing more basis functions where Hamiltonian matrix diagonalization remains the main computational bottleneck in variational calculations.

Looking ahead, a natural extension of this work involves developing a more general, trainable coordinate mapping that embeds molecular parameters directly into the model.

DATA AVAILABILITY

The data that support the findings of this study are available within the article and through the repository: <https://gitlab.desy.de/CMI/CMI-public/flows/-/releases/v.0.2.0>.

CODE AVAILABILITY

The code utilized and further developed in this work is publicly available at <https://gitlab.desy.de/CMI/CMI-public/flows/-/releases/v.0.2.0>.

NOTES

The authors declare no competing financial interest.

ACKNOWLEDGMENTS

The authors would like to acknowledge Jochen Küpper and the CFEL Controlled Molecule Imaging group for valuable scientific discussion and organisational support. The authors also acknowledge Henrik G. Kjaergaard for useful comments on the manuscript.

This work was supported by Deutsches Elektronen-Synchrotron DESY, a member of the Helmholtz Association (HGF), including the Maxwell computational resource operated at DESY, by the Data Science in Hamburg HELMHOLTZ Graduate School for the Structure of Matter (DASHH, HIDSS-0002), and by the Deutsche Forschungsgemeinschaft (DFG) through the cluster of excellence “Advanced Imaging of Matter” (AIM, EXC 2056, ID 390715994). This project has received funding from the European Union’s Horizon Europe research and innovation programme under the Marie Skłodowska-Curie grant agreement No. 101155136.

- ¹B. J. Braams and J. M. Bowman, “Permutationally invariant potential energy surfaces in high dimensionality,” *Int. Rev. Phys. Chem.* **28**, 577–606 (2009).
- ²S. Manzhos and T. Carrington, “Neural network potential energy surfaces for small molecules and reactions,” *Chem. Rev.* **121**, 10187 (2021).
- ³I. I. Mizus, A. A. Kyuberis, N. F. Zobov, V. Y. Makhnev, O. L. Polyansky, and J. Tennyson, “High-accuracy water potential energy surface for the calculation of infrared spectra,” *Philosophical Transactions of the Royal Society A: Mathematical, Physical and Engineering Sciences* **376**, 20170149 (2018).
- ⁴Y. Saleh, V. Sanjay, A. Iske, A. Yachmenev, and J. Küpper, “Active learning of potential-energy surfaces of weakly bound complexes with regression-tree ensembles,” *J. Chem. Phys.* **155**, 144109 (2021), arXiv:2104.00708 [physics].
- ⁵J. M. Bowman, S. Carter, and X. Huang, “MULTIMODE: A code to calculate rovibrational energies of polyatomic molecules,” *Int. Rev. Phys. Chem.* **22**, 533–549 (2003).
- ⁶P. R. Franke, J. F. Stanton, and G. E. Doublerly, “How to VPT2: Accurate and intuitive simulations of CH stretching infrared spectra using VPT2+K with large effective hamiltonian resonance treatments,” *J. Phys. Chem. A* **125**, 1301–1324 (2021).
- ⁷M. B. Hansen, M. Sparta, P. Seidler, D. Toffoli, and O. Christiansen, “New formulation and implementation of vibrational self-consistent field theory,” *J. Chem. Theory Comput.* **6**, 235–248 (2009).
- ⁸S. N. Yurchenko, W. Thiel, and P. Jensen, “Theoretical ROVibrational Energies (TROVE): A robust numerical approach to the calculation of rovibrational energies for polyatomic molecules,” *J. Mol. Spectrosc.* **245**, 126–140 (2007).
- ⁹E. Mátyus, G. Czakó, and A. G. Császár, “Toward black-box-type full- and reduced-dimensional variational (ro)vibrational computations,” *J. Chem. Phys.* **130**, 134112 (2009).
- ¹⁰M. J. Bramley, W. H. Green, and N. C. Handy, “Vibration-rotation coordinates and kinetic energy operators for polyatomic molecules,” *Mol. Phys.* **73**, 1183–1208 (1991).
- ¹¹M. Mendolicchio, J. Bloino, and V. Barone, “Perturb-then-diagonalize vibrational engine exploiting curvilinear internal coordinates,” *J. Chem. Theory Comput.* **18**, 7603–7619 (2022).
- ¹²E. Mátyus, A. M. S. Daría, and G. Avila, “Exact quantum dynamics developments for floppy molecular systems and complexes,” *Chem. Comm.* **59**, 366–381 (2023).
- ¹³Z. Bačić and J. C. Light, “Theoretical methods for rovibrational states of floppy molecules,” *Annu. Rev. Phys. Chem.* **40**, 469–98 (1989).
- ¹⁴I. Simkó, C. Schran, F. Briec, C. Fábri, O. Asvany, S. Schlemmer,

- D. Marx, and A. G. Császár, “Quantum nuclear delocalization and its rovibrational fingerprints,” *Angew. Chem. Int. Ed.* **62**, e202306744 (2023).
- ¹⁵A. Yachmenev and S. N. Yurchenko, “Automatic differentiation method for numerical construction of the rotational-vibrational Hamiltonian as a power series in the curvilinear internal coordinates using the Eckart frame,” *J. Chem. Phys.* **143**, 014105 (2015).
- ¹⁶X.-G. Wang and T. Carrington, “Vibrational energy levels of CH_5^+ ,” *J. Chem. Phys.* **129**, 234102 (2008).
- ¹⁷F. Gatti, C. Iung, M. Menou, Y. Justum, A. Nauts, and X. Chapuisat, “Vector parametrization of the N-atom problem in quantum mechanics. I. Jacobi vectors,” *J. Chem. Phys.* **108**, 8804–8820 (1998).
- ¹⁸C. Leforestier, A. Viel, F. Gatti, C. Muñoz, and C. Iung, “The Jacobi–Wilson method: A new approach to the description of polyatomic molecules,” *J. Chem. Phys.* **114**, 2099–2105 (2001).
- ¹⁹M. J. Bramley and N. C. Handy, “Efficient calculation of rovibrational eigenstates of sequentially bonded four-atom molecules,” *J. Chem. Phys.* **98**, 1378–1397 (1993).
- ²⁰Z. Bačić, R. B. Gerber, and M. A. Ratner, “Vibrational levels and tunneling dynamics by the optimal coordinates, self-consistent field method: A study of hydrocyanic acid. dblarw. hydroisocyanic acid,” *J. Chem. Phys.* **90**, 3606–3612 (1986).
- ²¹X. Chapuisat, A. Nauts, and J.-P. Brunet, “Exact quantum molecular hamiltonians,” *Mol. Phys.* **72**, 1–31 (1991).
- ²²C. Iung and F. Gatti, “Polyspherical parametrization of an N-atom system: Principles and applications,” *Int. J. Quantum Chem.* **106**, 130–151 (2005).
- ²³F. Gatti and C. Iung, “Exact and constrained kinetic energy operators for polyatomic molecules: The polyspherical approach,” *Phys. Rep.* **484**, 1–69 (2009).
- ²⁴E. L. Klinting, D. Lauvergnat, and O. Christiansen, “Vibrational coupled cluster computations in polyspherical coordinates with the exact analytical kinetic energy operator,” *J. Chem. Theory Comput.* **16**, 4505–4520 (2020).
- ²⁵J. M. Bowman, T. Carrington, and H.-D. Meyer, “Variational quantum approaches for computing vibrational energies of polyatomic molecules,” *Mol. Phys.* **106**, 2145–2182 (2008).
- ²⁶T. C. Thompson and D. G. Truhlar, “Optimization of vibrational coordinates, with an application to the water molecule,” *J. Chem. Phys.* **77**, 3031–3035 (1982).
- ²⁷R. C. Mayrhofer and E. L. Sibert, “Investigating optimal coordinates for describing vibrational motion,” *Theor. Chim. Acta* **92**, 107–122 (1995).
- ²⁸K. Oenen, D. F. Dinu, and K. R. Liedl, “Determining internal coordinate sets for optimal representation of molecular vibration,” *J. Chem. Phys.* **160**, 014104 (2024).
- ²⁹D. Mendive-Tapia, H.-D. Meyer, and O. Vendrell, “Optimal mode combination in the multiconfiguration time-dependent hartree method through multivariate statistics: Factor analysis and hierarchical clustering,” *J. Chem. Theory Comput.* **19**, 1144–1156 (2023).
- ³⁰M. Schneider and G. Rauhut, “Comparison of curvilinear coordinates within vibrational structure calculations based on automatically generated potential energy surfaces,” *J. Chem. Phys.* **161**, 094102 (2024).
- ³¹J. Zúñiga, J. A. G. Picón, A. Bastida, and A. Requena, “On the use of optimal internal vibrational coordinates for symmetrical bent triatomic molecules,” *J. Chem. Phys.* **122**, 224319 (2005).
- ³²J. M. Bowman, J. Zúñiga, and A. Wierzbicki, “Investigations of transformed mass-scaled Jacobi coordinates for vibrations of polyatomic molecules with application to H_2O ,” *J. Chem. Phys.* **90**, 2708–2713 (1989).
- ³³K. Yagi, M. Keçeli, and S. Hirata, “Optimized coordinates for anharmonic vibrational structure theories,” *J. Chem. Phys.* **137**, 204118 (2012).
- ³⁴B. Thomsen, K. Yagi, and O. Christiansen, “Optimized coordinates in vibrational coupled cluster calculations,” *J. Chem. Phys.* **140**, 154102 (2014).
- ³⁵B. Ziegler and G. Rauhut, “Localized normal coordinates in accurate vibrational structure calculations: Benchmarks for small molecules,” *J. Chem. Theory Comput.* **15**, 4187–4196 (2019).
- ³⁶X.-G. Wang and T. Carrington, “A discrete variable representation method for studying the rovibrational quantum dynamics of molecules with more than three atoms,” *J. Chem. Phys.* **130**, 094101 (2009).
- ³⁷J. Hermann, Z. Schätzle, and F. Noé, “Deep-neural-network solution of the electronic Schrödinger equation,” *Nat. Chem.* **12**, 891–897 (2020).
- ³⁸D. Pfau, J. S. Spencer, A. G. D. G. Matthews, and W. M. C. Foulkes, “*Ab initio* solution of the many-electron Schrödinger equation with deep neural networks,” *Phys. Rev. Research* **2**, 033429 (2020).
- ³⁹Y. Saleh, Á. F. Corral, E. Vogt, A. Iske, J. Küpper, and A. Yachmenev, “Computing excited states of molecules using normalizing flows,” preprint (2023), arXiv:2308.16468 [physics].
- ⁴⁰G. Papamakarios, E. Nalisnick, D. J. Rezende, S. Mohamed, and B. Lakshminarayanan, “Normalizing flows for probabilistic modeling and inference,” *J. Mach. Learn. Res.* **22**, 2617–2680 (2022).
- ⁴¹J. Behrmann, W. Grathwohl, R. T. Q. Chen, D. Duvenaud, and J.-H. Jacobsen, “Invertible residual networks,” in *Proceedings of the 36th International Conference on Machine Learning*, Proceedings of Machine Learning Research, Vol. 97, edited by K. Chaudhuri and R. Salakhutdinov (PMLR, 2019) pp. 573–582.
- ⁴²Q. Zhang, R.-S. Wang, and L. Wang, “Neural canonical transformations for vibrational spectra of molecules,” *J. Chem. Phys.* **161**, 024103 (2024).
- ⁴³Q. Zhang, X. Wang, R. Shi, X. Ren, H. Wang, and L. Wang, “Neural canonical transformations for quantum anharmonic solids of lithium,” (2024), arXiv:2412.12451 [cond-mat.mtrl-sci].
- ⁴⁴Y. Saleh and A. Iske, “Inducing Riesz and orthonormal bases in L^2 via composition operators,” preprint (2024), arXiv:2406.18613 [math].
- ⁴⁵DeepMind, I. Babuschkin, K. Baumli, A. Bell, S. Bhupatiraju, J. Bruce, P. Buchlovsky, D. Budden, T. Cai, A. Clark, I. Danihelka, A. Dedieu, C. Fantacci, J. Godwin, C. Jones, R. Hemsley, T. Hennigan, M. Hessel, S. Hou, S. Kapturovski, T. Keck, I. Kemaev, M. King, M. Kunesch, L. Martens, H. Merzic, V. Mikulik, T. Norman, G. Papamakarios, J. Quan, R. Ring, F. Ruiz, A. Sanchez, L. Sartran, R. Schneider, E. Sezener, S. Spencer, S. Srinivasan, M. Stanojević, W. Stokowiec, L. Wang, G. Zhou, and F. Viola, “The DeepMind JAX Ecosystem,” (2020).
- ⁴⁶P. M. Morse, “Diatomic molecules according to the wave mechanics. II. vibrational levels,” *Phys. Rev.* **34**, 57–64 (1929).
- ⁴⁷E. Vogt, D. S. Sage, and H. G. Kjaergaard, “Accuracy of XH-stretching intensities with the Deng-Fan potential,” *Mol. Phys.* **117**, 1629–1639 (2019).
- ⁴⁸A. A. A. Azzam, J. Tennyson, S. N. Yurchenko, and O. V. Naumenko, “ExoMol molecular line lists – XVI. the rotation-vibration spectrum of hot H_2S ,” *Mon. Not. R. Astron. Soc.* **460**, 4063–4074 (2016).
- ⁴⁹E. K. Conway, I. E. Gordon, J. Tennyson, O. L. Polyansky, S. N. Yurchenko, and K. Chance, “A semi-empirical potential energy surface and line list for H_2^{16}O extending into the near-ultraviolet,” *Atmos. Chem. Phys.*, **20**, 10015–10027 (2020).
- ⁵⁰C. Lubich, *From quantum to classical molecular dynamics: reduced models and numerical analysis* (European Mathematical Society, 2008).
- ⁵¹Y. Saleh, *Spectral and active learning for enhanced and computationally scalable quantum molecular dynamics*, Dissertation, Universität Hamburg, Hamburg, Germany (2023).